

ASDF: Assembly State Detection Utilizing Late Fusion by Integrating 6D Pose Estimation

Hannah Schieber* Shiyu Li† Niklas Corell‡ Philipp Beckerle§ Julian Kreimeier¶ Daniel Roth||

Technical University of Munich
Human-Centered Computing and
Extended Reality Lab
TUM School of Medicine and Health
TUM School of Computation,
Information and Technology
Clinic for Orthopedics and
Sports Orthopedics
TUM University Hospital,
Munich, Germany^{*,†,¶,||}

Department Artificial Intelligence in
Biomedical Engineering
Friedrich-Alexander Universität (FAU)
Erlangen-Nürnberg
Erlangen, Germany^{‡,§}

Chair of Autonomous Systems and
Mechatronics
Friedrich-Alexander Universität (FAU)
Erlangen-Nürnberg
Erlangen, Germany[§]

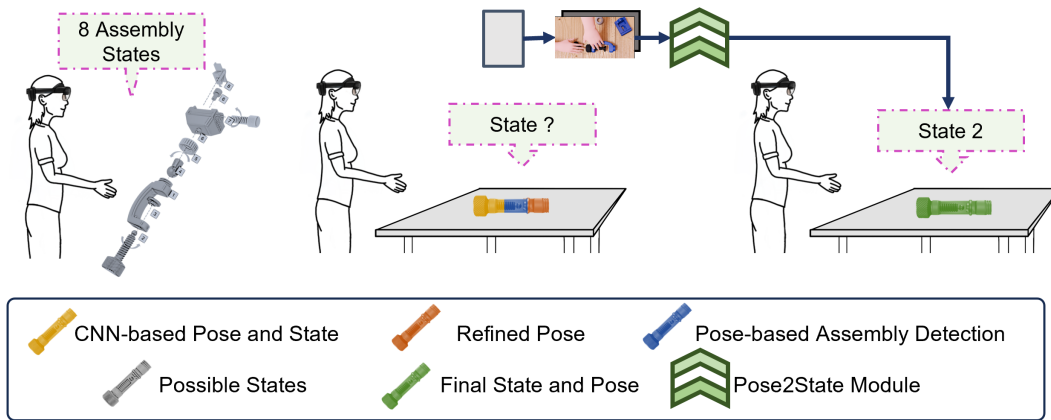


Figure 1: **We present assembly state detection utilizing late fusion (ASDF).** Our approach fuses RGB and depth information as well as 6D pose estimation and state predictions. In our Pose2State module we calculate the final state in a late fusion step by combining 6D pose estimation and assembly state detection.

ABSTRACT

In medical and industrial domains, providing guidance for assembly processes can be critical to ensure efficiency and safety. Errors in assembly can lead to significant consequences such as extended surgery times and prolonged manufacturing or maintenance times in industry. Assembly scenarios can benefit from in-situ augmented reality visualization, i.e., augmentations in close proximity to the target object, to provide guidance, reduce assembly times, and minimize errors. In order to enable in-situ visualization, 6D pose estimation can be leveraged to identify the correct location for an augmentation. Existing 6D pose estimation techniques primarily focus on individual objects and static captures. However, assembly scenarios have various dynamics, including occlusion during assembly and dynamics in the appearance of assembly objects. Existing work focus either on object detection combined with state

detection, or focus purely on the pose estimation. To address the challenges of 6D pose estimation in combination with assembly state detection, our approach ASDF builds upon the strengths of YOLOv8, a real-time capable object detection framework. We extend this framework, refine the object pose, and fuse pose knowledge with network-detected pose information. Utilizing our late fusion in our Pose2State module results in refined 6D pose estimation and assembly state detection. By combining both pose and state information, our Pose2State module predicts the final assembly state with precision. The evaluation of our ASDF dataset shows that our Pose2State module leads to an improved assembly state detection and that the improvement of the assembly state further leads to a more robust 6D pose estimation. Moreover, on the GBOT dataset, we outperform the pure deep learning-based network and even outperform the hybrid and pure tracking-based approaches.

Index Terms: 6D pose estimation, assembly state detection, synthetic data

1 INTRODUCTION

Providing error-free assembly of complex assembly groups is highly relevant in manufacturing, maintenance, or medical scenarios [4, 51, 19, 25]. Object assembly in these cases can be challenging due to the time pressure, the need for high accuracy, and the requirement for prior knowledge about the individual assem-

*e-mail: hannah.schieber@tum.de

†e-mail: shiyu.li@tum.de

‡e-mail: niklas.corell@fau.de

§e-mail: philipp.beckerle@fau.de

¶e-mail: julian.kreimeier@tum.de

||e-mail: daniel.roth@tum.de

bly parts. Moreover, assembly errors in manufacturing can lead to broken parts, extended manufacturing times or in the medical context this can affect the surgery time. Support during assembly tasks can reduce physiological and psychological loads in such scenarios [39, 11]. To support these scenarios, augmented reality (AR) guidance can provide valuable dynamic visualization during the assembly process. Enabling dynamic visualization for assembly processes requires accurate real-time tracking of the objects and their current state in the assembly. While markers proved high accuracy for tracking in AR they are sometimes not suitable for every task in manufacturing or medical scenarios [4]. An alternative approach to markers in AR, is the utilization of 6D pose estimation of assembly objects [21]. Deep learning-driven 6D pose estimation determines both the position and orientation of objects in three-dimensional space, enabling markerless tracking.

To provide in-situ guidance, knowledge of the current assembly state is required along with each objects position in space. Retrieving this knowledge is especially challenging in dynamic assembly scenarios [51, 38]. Furthermore, existing 6D pose estimation approaches [45, 26] are often limited to static scenes [17, 46] as the benchmark on which they are evaluated are static. Alternatively, object tracking is more often applied in dynamic scenarios with moving objects [36, 35, 21], but occlusion can be challenging for pure tracking-based approaches [21]. AR assembly guidance combined with 6D pose estimation and state-detection can enable in-situ guidance, and error detection during the assembly to reduce risks and assembly time. Marker-based tracking, however, limits real-world applicability. To enable marker-less 6D pose estimation and state detection, using a deep learning-based approach can be beneficial.

In summary, existing deep learning-based multi-object approaches a) limit their object and state detection to 2D [23, 32, 53], b) limit their evaluation to one or two objects [23, 25], or c) only provide the 6D object pose information without predicting the current assembly state [21, 33, 36].

To address these limitations, we present assembly state detection utilizing late fusion (ASDF), a deep learning-based system for assembly state detection and 6D pose estimation. We build upon the real-time capable you only look once (YOLO) architecture, fusing 6D pose estimation and assembly state detection for more precise object poses. Additionally, we propose a fully synthetic dataset for training and evaluation, with an additional real-world test scene. Our ASDF dataset consists of online available 3D printing parts with 6D pose estimation ground truth and assembly state ground truth. The test dataset contains full assembly sequences with hand occlusion and faulty states for a robust evaluation. We evaluate various aspects, such as network size and pose refinement, on our ASDF dataset.

Furthermore, we compare our approach’s 6D pose estimation performance on the graph-based object tracking (GBOT) dataset [21]. This evaluation demonstrates the transferability of our domain-randomized training images to the GBOT evaluation images and shows that assembly state detection can enhance 6D pose performance.

In summary, we contribute:

- ASDF, a late fusion approach enhancing assembly state detection and 6D pose estimation through improved assembly state prediction
- Our synthetic ASDF dataset that includes 6D object poses and assembly states using 3D printable parts for reproducibility¹
- State-of-the-art results on two datasets with assembly assets, demonstrating the advantage of our approach

¹GitHub ASDF

2 RELATED WORK

2.1 6D Object Pose Estimation and Tracking

Instance-level 6D pose estimation can be divided in one-stager [10, 49] and two-stager [45] approaches. One-stagers are end-to-end trainable [10, 49]. They extract features from a segmentation or object detection backbone. These can be regressed directly [49] or other output like keypoints can be feed to perspective-n-point (PnP) [40]/Least Squares Fitting [10]. Amini et al. [2] introduce YoloPose which directly regresses keypoints in an image and presents a learnable module to replace PnP. Two-stagers, apply a state-of-the-art object detection algorithm, for example Faster R-CNN [8] and build the 6D pose estimation on top of these predictions. Wang et al. [45] utilize geometric feature regression on top of the object detection algorithm. This results in 2D-3D correspondences and Surface Region Attention which is leveraged in Patch-PnP. Similarly, Pix2Pose [26] leverages 2D bounding boxes followed by mask prediction step and bounding box refinement step. The final result is predicted using RANSAC PnP [7, 20, 52]. While one-stagers are often more computationally cheap during inference time, two-stagers can provide more accuracy.

In addition to deep learning-based 6D pose estimation, another crucial field for AR-driven instructions and object-based applications is object tracking [44]. Object tracking starts with a pose initialization and then assumes the 6D object pose in the following frames. Stoiber et al. [36] combine visual, regions and depth information. Their improvement ICG+ [33] additionally considers SIFT and ORB features. For objects consisting of multiple parts, Mb-ICG [35] looked at kinematic structures. However, they track the complete assembled object instead of the individual assembly steps. Object tracking can get lost in highly occluded scenes. Li et al. [21] propose a combination of an extension of YOLOv8 and an improvement of iterative correspondence geometry (ICG) to re-initialize the tracking if it gets lost. While their pose initialization relies on the convolutional neural network (CNN), they utilize an assembly state-graph for tracking assembled objects. Furthermore, they provide the GBOT dataset for tracking assembled parts.

2.2 Assembly State Detection for Augmented Reality

While the object pose is an essential aspect for assembly guidance another one is the assembly state itself. Zauner et al. [51] utilized markers and build an assembly graph for AR-based assembly instruction. *Duplotrack* [9] utilizes point cloud alignment whenever the assembly building blocks change. Radkowski et al. [28], utilize object tracking with iterative closest point (ICP)-based refinement for AR-guided assembly matching point clouds.

In terms of 2D assembly state detection, Kleinbeck et al. [19] combine YOLOv5 [16] and synthetic data for building block assembly guidance. The guidance steps are rendered in a Hololens. Similarly, Stanescu et al. [32] provide AR glasses-based guidance. For their state detection they introduce an extra convolution block in YOLO. Overall, their state detection improved the YOLO-based object prediction.

Liu et al. [23] integrate a two-fold attention mechanism in a 2D object detection architecture. They test their approach on two objects, an IKEA table assembly and Fender assembly. Zhou et al. [53] address mobile AR guidance utilizing regions-of-interest for state identification. The method is two-fold, in a first step the regions-of-interest are extracted, in a second step, the state recognition is trained.

Other approaches considering 3D/6D build upon the relative pose between objects [24, 25, 48]. Wu et al. [48] follow a tree like graph structure to determine the assembly state. Similarly, Murray et al. [25] address 6D pose estimation and assembly prediction for robot bin picking defining an assembly state graph. They omit training object detection as a first stage since they are dealing with one single object in front of the camera. For 6D pose estimation

they follow Pix2Pose [26] and address multi-view input utilizing depth estimation and project pixels to 3D. Su et al. [38] utilize a TridentNet as backbone and add a pose prediction head. They predict the pose and assembly state for one object with five assembly states and provide AR guidance for utilizing the network.

2.3 Real-world and Synthetic Datasets

For 6D pose estimation/object tracking multiple benchmarks exist, for example, one common benchmark is the YCB-V benchmark [49]. However, this and other common ones considers single objects without state changes [3, 49, 17, 15]. Moreover, providing 6D pose datasets with complex scenes and switching object states is challenging. To address this challenge, one common approach is the use of synthetic data [29, 25, 21].

2.3.1 Assembly State Datasets

One common area for assembly datasets is IKEA furniture [47, 37, 23]. The IKEA-Manual dataset [47] provides assembly data including the 3D pose of each part, specifically detailing the rotation of the 3D components. However, it does not explore the translation of individual parts. Addressing this limitation, the IKEA assembly dataset [37] fills the gap, although it is not publicly accessible.

Other works build upon individual objects [25, 38, 32]. However, this makes reproducibility more challenging. Schoonbeek et al. [30] present a hybrid multi-modal dataset focusing on action recognition recorded with a Hololens 2. Su et al. [38] reconstruct a real-world coffee machine and sample the parts on images to generate a synthetic assembly state dataset.

For reproducibility, Li et al. [21] propose the use of 3D printable objects and present a synthetic dataset featuring these objects and their poses. The individual objects have a varying number of assembly states and different sizes.

2.3.2 Synthetic Data

The use of synthetic data for 6D position estimation can be useful as obtaining a real markerless dataset is a challenging task [17, 29, 41]. The use of synthetic data poses the challenge of the so-called sim-to-real gap [29, 42]. This gap refers to the domain gap between synthetic and real images. To close this gap, various parameters such as light, background, object textures are often randomized and distracting objects are added [29, 43, 1]. Tremblay et al. [43] investigated this by combining realistic and randomized images and adding distractor objects. This increased the performance of object recognition. Alghonhaim et al. [1] tested domain randomization considering background, textures and distractors. They also proved that distractors are beneficial for the generalization of a CNN.

The constant progress in 6D pose estimation is promising for single objects [45, 40, 27, 26, 10, 50], the combination of 6D pose estimation and assembly state detection is even more promising for AR guidance approaches [21, 25]. However, for these tasks the used objects hugely vary from building blocks [39, 19, 32] up to engines with over a hundred assembly states [25]. Existing approaches are often limited to 2D [32], omit training an object detection model in the first stage [25], require additional state recognition in addition to their robust object tracking [21] or can not handle state switches [35]. To address these limitations we propose ASDF an end-to-end approach for assembly state detection and 6D pose estimation. Moreover, existing datasets for this task are again either for 2D object detection, 6D pose estimation [21], limited to action recognition [31] or not publicly available. To enhance comparison in this area we propose our ASDF dataset containing 6D object pose ground and assembly state truth data using 3D printable object’s for comparability and reproducibility.

3 METHOD

3.1 Assembly State Detection Utilizing Late Fusion

ASDF estimates both the 6D pose and the assembly state, which we will explain separately. The individual outputs are fused in a late fusion step within our Pose2State module.

3.1.1 6D Pose Estimation

ASDF uses RGB-D images. The backbone processes the pure RGB image. The Translation Refinement module utilizes the depth image and resulting point cloud to refine the pose, see Figure 2.

For 6D pose estimation, we leverage YOLOv8Pose [21], an extension of YOLOv8 utilizing RANSAC PnP. To establish keypoints in 3D space, we utilize the 2D keypoints predicted by the backbone. Using farthest point sampling (FPS) [21, 27], we distribute the points as widely apart as possible. The selection of a final number of keypoints (17) creates a balance between computing costs and performance, as more keypoints increase the computing costs.

Assembly Pose Translation Refinement Our assembly pose refinement step enhances the estimated translation by identifying the boundary values of each assembly in every assembly group, see Figure 2. To accomplish this, we determine the necessary movement along one coordinate axis (the z-axis) and proportionally adjust the other two axes. To calculate this movement perpendicular to the camera plane, we transform the 3D surface points P_{3D} of the component using the transformation matrix obtained from the initial pose estimation by our CNN (T_{DL}).

The transformed points P'_{3D} of the 3D surface points P_{3D} using T_{DL} can be expressed as follows:

$$P'_{3D} = P_{3D} \cdot T_{DL} \quad (1)$$

Next, we back-project these points onto the 2D image plane (P_{2D}) and filter them using the predicted bounding box, resulting in visible points (P'_{2D}). Subsequently, through a second filtering process, we reduce the number of keypoints to those closest to the camera plane. Based on the 2D points, we approximate the depth information using the depth input. This results in approximated 3D points.

Finally, based on the selected points in P'_{2D} and the approximated depth, we determine the necessary movement along one coordinate axis (i.e., z) and proportionally adjust the other two axes (i.e., x and y) to refine the translation part. By utilizing the approximated 3D points, we calculate the difference from the corresponding 3D surface points. This allows us to estimate the shift for all points using:

$$E = \sum_{i=1}^n W(d_i) \cdot d_i \quad (2)$$

d_i denotes the estimated shift distance for point i and n represents the total number of points. E is the overall estimate of the required shift for all points.

To estimate the shift distance for each point, we use d_i . Then, to obtain an overall estimate, we combine these individual estimations using a weighting function $W(d_i)$. This function assigns higher weights to points with smaller differences, thereby preventing occluded objects from influencing false calculations during the refinement step.

The resulting translation along the axis perpendicular to the image plane can now be utilized to determine the vector along the camera view axis, representing the final translation.

3.1.2 Assembly State Detection

The final assembly state detection combines three key components: deep learning-based state detection, relative pose-based state detection, and consideration of the previous state using a weighted late fusion.

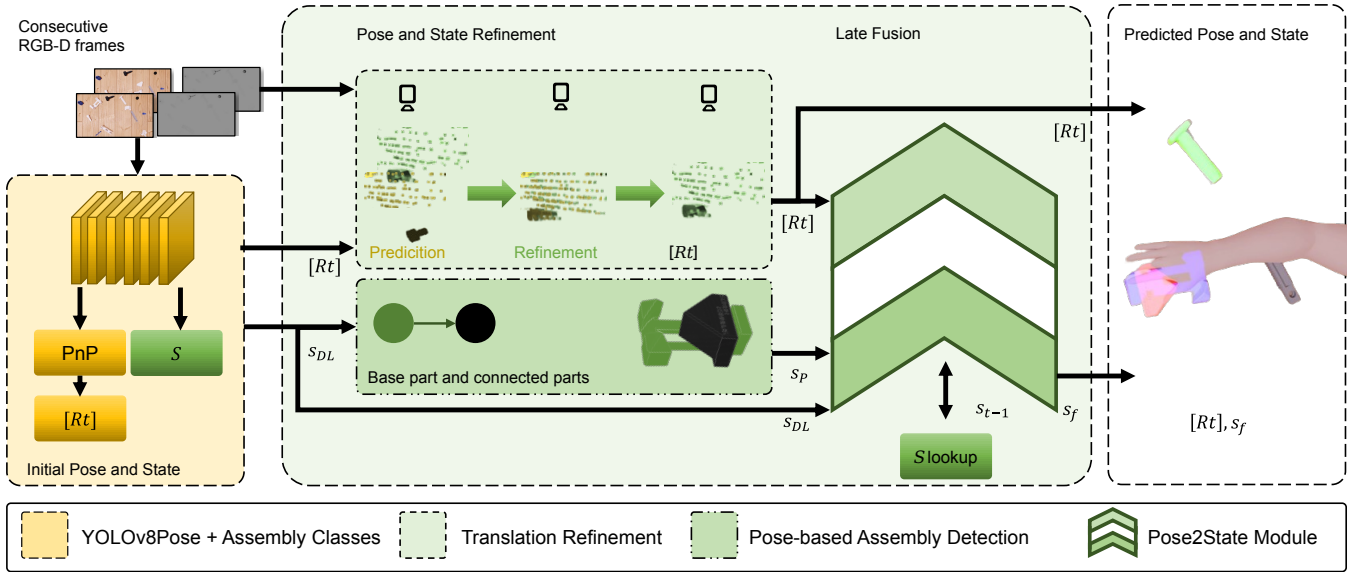


Figure 2: **Architecture of ASDF**. We highlight our contribution in green. ASDF utilizes RGB and depth data. The RGB images are fed into the image backbone and the depth data is used to refine the object poses ($[Rt]$). The image backbone predicts the state (s) based on the RGB image. In the Translation Refinement module, the translation offset is calculated. Using the relative pose between the assemblies in the assembly group, we predict a second state assumption in our Pose-based Assembly Detection module. In our final Pose2State module, we weight the individual state predictions to predict the one with the highest probability.

Deep learning-based Assembly State Detection The relationship between assembly state and 6D pose estimation is interdependent. Each pose of an assembly part within a group contributes valuable information to the overall assembly state, and conversely, the current assembly state informs the relative poses of the objects to each other.

To integrate state detection in ASDFs backbone, we represent each state as a distinct class. The assembled parts with a new assembly state are regarded as a new class.

Pose-based Assembly State Detection The relative position between objects provides valuable information about the current assembly state of each assembly. These relative poses are known because they are crucial for the creation of training and evaluation data.

To determine the assembly state based on the relative pose of an assembly, we select the base part of each assembly. Followed by this, we can interpret the relative poses of the entire assembly.

3.1.3 Pose2State Module

Given the inherent co-dependency between pose and state, we harness this relationship in our Pose2State module in a late fusion manner. This module is designed to forecast the state probability (SP) of the assembly state s_x at time t . Our Pose2State module seamlessly integrates two key components: the deep learning-based prediction (SP_{DL}) and the prediction derived from the pose-based assembly (SP_P). By combining these predictions, our module effectively determines the final assembly state, leveraging both deep learning and the pose-based assembly state.

We first combine the deep learning-based state prediction (SP_{DL}) and the pose-based state prediction (SP_P):

$$SP_{DL+P}(s_x)_t = w_{DL} \cdot P_{DL}(s_x)_t + w_P \cdot P_P(s_x)_t \quad (3)$$

For the final assembly state SP_f we consider the time component and leverage the previously stored assembly state ($(s_x)_{t-1}$). $P_f(s_{x\pm 1})_{t-1}$ represents the average normalised probability of the two neighbouring states $s_{x\pm 1}$ from the previous time step ($t-1$).



Figure 3: Assembly state complexity of the **ASDF dataset (left)** and **training images of the ASDF dataset (right)**. For training we use assembled and unassembled data (right) and additionally provide hand occlusion (top-right), varying background and light conditions as well as distracting objects. We include the state information in our ground truth labels. An example of the state complexity can be seen in the left figure.

$$SP_{f+f_{i-1}}(s_x)_t = w_f \cdot P_f(s_x)_{t-1} + w_{f-1} \cdot P_f(s_{x\pm 1})_{t-1} \quad (4)$$

This results in the probability (P) for the final assembly state $SP_{f+f_{i-1}}(s_x)_t$ at time t . We fuse the state probability (SP) our deep learning-based and relative-pose based estimation ($SP_{f+f_{i-1}}(s_x)_t$) and weight them:

$$P_f(s_x)_t = \frac{SP_{DL+P}(s_x)_t + SP_{f+f_{i-1}}(s_x)_t}{w_{DL} + w_P + w_f + w_{f-1}} \quad (5)$$

3.2 Assembly State Dataset

To address assembly states and 6D pose estimation, we created a synthetic dataset² with 3D-printed parts to facilitate testing under real conditions. We used the 3D printable parts from the GBOT

²GitHub ASDF

Table 1: **Number of states and synthetic test images for each assembly part.** The assembly groups of our ASDF dataset (left column), the number of states (center column), and number of images in the test set.

Assembly	No. States	Number of images
NanoVise	8	191
ScrewClamp	10	231
GearedCaliper	5	111
CornerClamp	3	66



Figure 4: **Example images with highlighted ground truth of our ASDF test set.** Synthetic image (left) and real-world image (right). The ground truth of each currently evaluated assembly group is visualized with colorful overlays.

dataset [21] as a foundation. In addition to the existing reproducible setup [21], we introduced assembly state information, wrong assembly states and incorporated hand occlusion during training to enhance the model’s robustness. Our dataset adheres to the camera specifications of the Azure Kinect DK, with a resolution set to 1280×720 pixels. The camera is positioned in a top-down view to simulate a capturing setup commonly found in medical or industrial scenarios.

3.2.1 Synthetic Dataset

Training and Validation Dataset Our synthetic dataset includes 6D pose estimation and assembly state detection ground truth data with 20k images per assembly, using an 80:20 training split. For testing each test scene contains a various number of images with several levels of domain randomization, see Table 1. Our dataset is generated using BlenderProc [6]. Domain randomization is crucial in synthetic data generation [29, 1]. Thus, we introduce distracting objects [13, 18] and simulate hand occlusion to reflect real-world scenarios, as shown in Figure 4. In addition to, to distracting objects and hand occlusion, we add randomized noise, different lighting variations, and varying background materials [1, 29].

Test Dataset For each assembly we generate a continuous sequence of assembly images resulting in a full assembly video. The test scenes contain one full assembly sequence including error states to test the robustness of the assembly state detection. We maintain the presence of distracting objects and incorporate hands at realistic assembly positions to mimic occlusion and test robustness. The objects are randomly distributed within the camera’s field of view. Each frame contains assembly state and 6D pose ground truth data.

A key aspect of our test set is the inclusion of incorrectly assembled states. In a real-world assembly scenario mounting together parts with missing pieces in between can happen especially if the parts are not necessarily connecting parts. Therefore, we added incorrect assembly states to test robustness. Since each object contains various assembly states, the number of evaluation images per assembly object varies, as illustrated in Table 1. This variability ensures comprehensive testing of the model’s ability to detect and handle different assembly scenarios.

4 EVALUATION

To benchmark the accuracy of the assembly state detection and 6D pose estimation, we evaluate our approach on our ASDF dataset and on the GBOT [21] datasets. Other comparisons with existing assembly state detection approaches [32, 23] in 2D are not possible, since both pose and state are relevant for the final prediction. Other works focus purely on state changes [31], purely on 6D pose performance [21] or build upon non publicly available [38, 25] assets or data.

GBOT Dataset: The GBOT dataset [21] is a exclusively a synthetic dataset designed for 6D object pose/tracking tasks. It comprises 3D printable assembly parts and contains five evaluation sequences, each presenting different levels of difficulty for object tracking (normal (N), dynamic (D), hand occlusion (H), and blur (B)). Utilizing the GBOT dataset, we conduct a comprehensive comparison of our approach against state-of-the-art methods in 6D pose estimation performance, particularly focusing on assemblies with dynamically changing states.

4.1 Implementation and Specifications

We trained our network for 300 epochs using early stopping. The training for all comparisons is executed on one machine with an Intel Core i9-10980XE CPU, 128 GB RAM and one NVIDIA GeForce RTX 3090 graphics card.

As loss term, we follow YOLOv8 combining the class-wise loss (L_{cls}), bounding box loss (L_{box}), the task-specific loss (L_{tsk}) all weighted by λ .

L_{tsk} is comprised of the pose loss (L_{pose}) which is defined as $L_{pose} = \|\mathbf{K}_{pred} - \mathbf{K}_{gr}\|_2$. This is the L2 loss using the predicted keypoints (L_{pose}) from the ground truth keypoints (\mathbf{K}_{gr}) and the Cross-Entropy (CE) Loss using the keypoints.

$$L_{total} = \sum_{i,j,k} (\lambda_{cls} L_{cls} + \lambda_{box} L_{box} + \lambda_{tsk} L_{tsk}) \quad (6)$$

4.2 Metrics

We evaluate our approach based on two main aspects: 6D pose estimation and state detection. For pose prediction, we report the absolute translation (e_t) [14], rotation error e_r [14] and average distance error (ADD)(S) [12, 21]. ADD(S) describes the average distance error for asymmetric (ADD) and symmetric (ADD(S)).

For state detection accuracy, we calculate the F1 score. The F1 score is composed of the calculation of precision and recall for each state (s) and each assembly part (c).

Since our goal is to utilize our state and pose recognition, we also evaluate the runtime. For the runtime, we calculate the average value over all assembly objects.

4.3 ASDF Results

We evaluate performance trade-off using different networks sizes, pose accuracy considering various refinement steps and benchmark our final approach.

4.3.1 Performance Trade-off

Since ASDF leverages object pose information to refine the state, our initial focus lies on evaluating the pose performance. As depicted in Table 3, it is evident that the fastest network performance can be attained using the smallest network configuration, which is a rational expectation. As overall network architecture we build upon YOLOv8Pose [21]. However, the underlying image backbone can vary in terms of network size. As shown in Table 3, the individual size n, m, l and x1-p6 have all their individual advantages and disadvantages for the pose performance. m and l exhibit similar performance, whereas the x1-p6 architecture, serving as our underlying backbone, demonstrates the most favorable results in terms of rotation and translation errors.

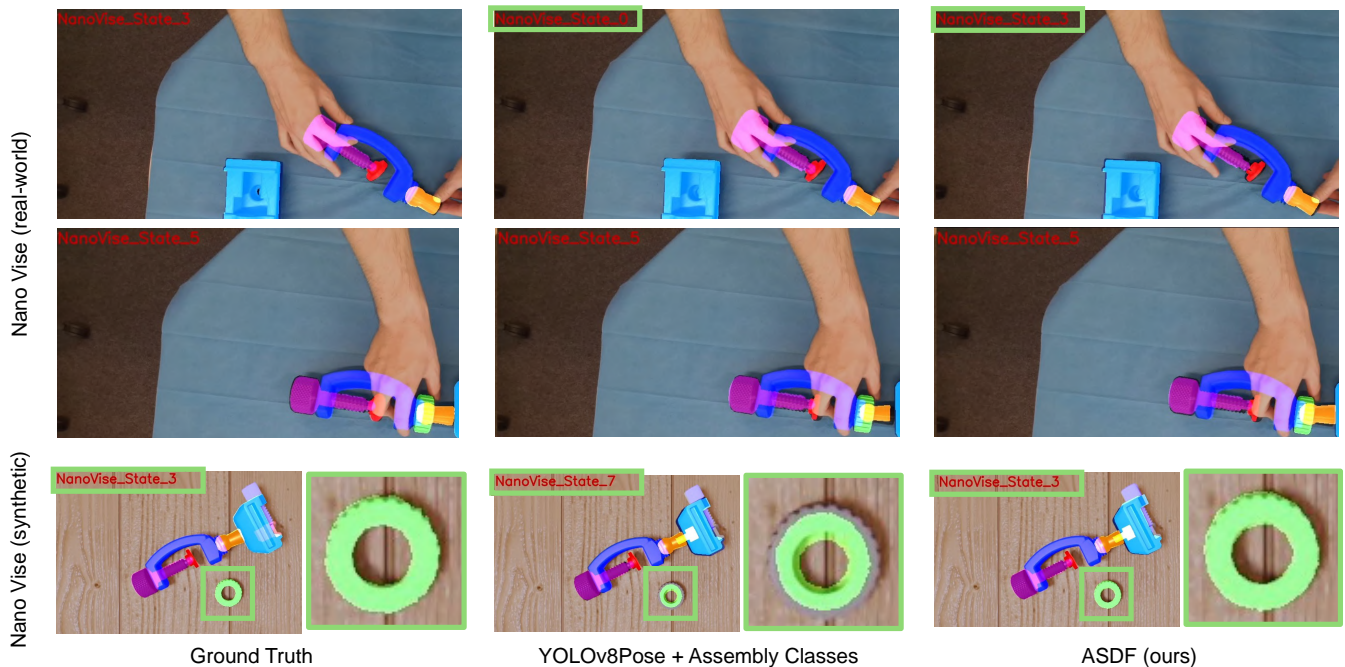


Figure 5: **Example of the results on the ASDF test set.** We show the performance of ASDF compared to YOLOv8Pose + Assembly Detection on real-world captures (top two lines) and synthetic renderings (bottom line). The ground truth (left), the pure YOLOv8-based pose and state prediction (center) and our prediction using ASDF (right). The current predicted state is denoted in every top-left corner and the pose is shown with a colorful overlays.

Table 2: **Ablation study on the impact of pose refinement steps and runtime on our ASDF dataset.** We compare our keypoint-based ASDF with YoloV8Pose + State + ICP (ICP-based refinement), and use an additional YOLO-based segmentation network for refinement (+ Seg). We provide a comparison using the smallest backbone (n) and the final backbone of ASDF (x1-p6). The best performing approach per category is **bold**.

Method	Backbone	Runtime [ms] ↓	e_{trans} ↓ [mm] ↓	erot [°] ↓
<i>No refinement</i>				
YOLOv8Pose + state	n	24.83	29.13	18.76
YOLOv8Pose + state	x1-p6	50.83	19.11	11.14
<i>ICP refinement</i>				
YOLOv8Pose + state + ICP	n	151.77	12.27	18.96
YOLOv8Pose + state + ICP	x1-p6	145.76	9.24	14.35
<i>Segmentation refinement</i>				
ASDF + Seg	n	64.46	8.52	18.76
ASDF + Seg	x1-p6	85.03	6.53	11.14
<i>Ours</i>				
ASDF	n	32.45	8.13	18.76
ASDF	x1-p6	55.70	5.98	11.14

Table 3: **Ablation study on the impact of the underlying network size on the pose accuracy.** We compare the individual backbone network sizes of YOLOv8Pose. As metrics we report runtime in ms and pose translation error in mm and rotation error in degree on the ASDF dataset. The best performing approach per category is **bold**.

Backbone	Runtime [ms] ↓	e_{trans} ↓ [mm] ↓	erot [°] ↓
n	24.83	29.13	18.76
m	33.72	27.85	15.21
l	35.55	23.69	13.09
x1-p6	50.83	19.11	11.14

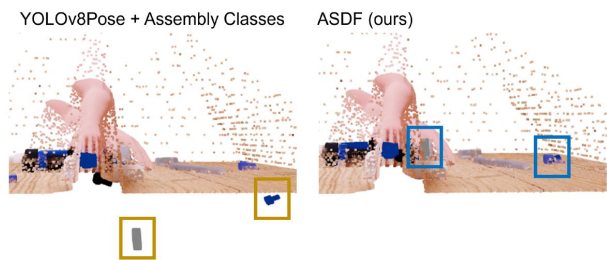


Figure 6: **Example comparison of the translation offset using YOLOv8Pose and ASDF.** YOLOv8Pose shows an offset in 3D (left, yellow) while the translation refinement of our ASDF (right, blue) can address this shift.

4.3.2 Pose Refinement

The backbone n shows the best runtime and the network size x1-p6 the best performance, see Table 3. Therefore, we further compared these two backbones considering different pose refinement methods. ASDF builds upon the use of keypoints for the 6D pose estimation. However, we considered other refinement methods as well to lift the pose performance. In Table 2 we compare the pure YOLOv8pose combined with the state prediction with the commonly used ICP-based refinement (YOLOv8pose + state + ICP). Additionally, since semantic segmentation provides clearer object boundaries, we compared our keypoint-based approach using a refinement step with a second YOLOv8 [16] semantic segmentation network and our ASDF with the backbones n and x1-p6.

The improvement of our translation refinement compared to the pure network-based output can be seen in Figure 6 and in Table 3. As shown in Table 2 neither the additional segmentation network nor ICP-based pose refinement can outperform ASDF.

Table 4: **Results on the ASDF dataset:** The ADD(S)(\uparrow) is calculated with 10cm threshold, the translation error is in millimeters (mm) denoted as e_{trans} [mm], (\downarrow) and the rotation error denoted as e_{rot} [$^\circ$], (\downarrow) in degrees. The best results among all methods are labeled in **bold**. We compare YOLOv8Pose using deep learning-based state detection with ASDF. To report the state performance we report the F1 score.

Assembly	YOLOv8Pose + Assembly Classes				ASDF			
	F1 \uparrow	ADD(S) \uparrow	e_{trans} [mm] \downarrow	e_{rot} [$^\circ$] \downarrow	F1 \uparrow	ADD(S) \uparrow	e_{trans} [mm] \downarrow	e_{rot} [$^\circ$] \downarrow
Corner Clamp	87.88	89.22	15.74	8.51	93.85	95.69	5.39	8.76
Screw Clamp	73.28	85.53	23.07	22.48	84.35	95.02	9.12	20.68
Geared Caliper	58.77	81.11	22.92	16.69	60.91	96.33	4.65	17.03
Nano Vise	75.45	83.82	21.88	5.04	78.95	95.92	7.63	8.22
Mean	73.85	84.92	20.90	13.18	79.52	95.74	6.70	13.67

Table 5: **Results on the GBOT dataset:** We compare our approach on the GBOT benchmark with the four conditions normal (N), dynamic (D), hand (H) and blur (B). We compare against their pure deep learning-based approach, the combined approach of deep learning and object tracking (GBOT + re-init) and pure tracking-based approaches. Rotational errors are only evaluated for unsymmetrical objects. The ADD(S)(\uparrow) is calculated with 10cm threshold, the translation error is in millimeters (mm) ($e_{ave,trans}$ denoted as e_{trans} , \downarrow) and the rotation error ($e_{ave,rot}$ denoted as e_{rot} , \downarrow) in degrees. The best results among all methods are labeled in bold. In this evaluation, tracking is initialized with ground truth pose only for the first frame and the pose is not reinitialized afterwards. In the last column, the tracking results of tracking re-initialization by pose estimation are shown.

Approach		6D pose estimation						Tracking						6D pose estimation + tracking								
Asset	Condition	ASDF (ours)			YOLOv8Pose [21]			SRT3D [34]			ICG [36]			ICG+SRT3D [22]			GBOT [21]			GBOT + re-init [21]		
		ADD(S)	e_{trans} [mm]	e_{rot} [$^\circ$]	ADD(S)	e_{trans} [mm]	e_{rot} [$^\circ$]	ADD(S)	e_{trans} [mm]	e_{rot} [$^\circ$]	ADD(S)	e_{trans} [mm]	e_{rot} [$^\circ$]	ADD(S)	e_{trans} [mm]	e_{rot} [$^\circ$]	ADD(S)	e_{trans} [mm]	e_{rot} [$^\circ$]	ADD(S)	e_{trans} [mm]	e_{rot} [$^\circ$]
Corner Clamp	N	100.0	18	3.0	91.5	93	3.8	89.8	47	25.8	100.0	1	38.7	100.0	13	38.7	100.0	6	2.1	99.5	7	2.7
	D	100.0	18	2.7	99.0	25	4.8	88.4	37	25.0	100.0	15	46.8	100.0	20	47.8	100.0	6	23.2	100.0	5	3.5
	H	68.6	83	38.4	45.4	541	97.1	66.6	88	37.1	68.4	74	59.4	68.4	75	58.3	81.9	57	90.4	90.6	44	84.7
	B	100.0	19	3.4	97.3	40	4.3	88.9	50	30.4	100.0	5	2.2	100.0	10	3.0	100.0	6	2.1	99.9	6	2.1
Geared Caliper	N	100.0	4	4.7	99.6	14	10.1	90.6	18	5.4	100.0	2	2.6	100.0	3	3.0	100.0	2	2.1	100.0	5	3.3
	D	100.0	3	4.1	99.9	13	9.3	92.7	14	9.9	100.0	2	2.5	100.0	0.4	3.6	100.0	0.2	2.3	100.0	0.5	3.6
	H	100.0	8	6.9	99.2	24	12.5	96.5	9	4.4	85.4	30	30.0	85.5	31	30.0	85.4	30	30.0	99.6	8	7.0
	B	100.0	4	4.9	99.6	14	9.9	98.9	9	8.7	100.0	2	2.5	100.0	3	2.8	100.0	2	2.2	100.0	5	3.6
Nano Vise	N	100.0	14	4.8	71.1	88	4.8	74.1	66	13.8	89.8	21	16.7	89.4	23	16.5	99.8	6	7.2	93.8	24	3.6
	D	90.0	16	5.0	72.6	76	4.6	63.4	103	15.6	87.3	39	15.3	87.3	41	15.8	96.0	24	20.0	92.9	25	3.7
	H	98.6	19	5.3	65.9	110	4.7	61.4	136	15.3	76.5	60	18.3	75.8	61	18.1	72.9	87	14.5	87.8	31	7.3
	B	100.0	15	5.4	70.9	99	5.2	61.9	116	15.2	91.6	19	11.4	91.5	21	11.1	95.7	7	25.1	92.7	30	4.7
Screw Clamp	N	93.5	11	8.6	73.5	77	17.6	86.5	47	8.9	96.0	12	1.1	95.9	14	2.3	98.8	4	0.9	83.7	30	4.7
	D	94.5	11	9.4	82.0	67	18.4	86.4	56	27.0	95.9	17	2.1	95.9	22	3.4	98.8	6	1.7	91.6	21	6.1
	H	92.1	18	13.5	67.2	142	39.8	60.1	143	37.7	73.4	69	53.4	73.1	71	53.4	68.7	79	61.9	83.9	49	27.2
	B	96.1	9	8.7	85.6	65	18.6	86.5	56	34.6	95.7	30	6.6	95.7	32	7.7	98.6	12	1.1	91.1	30	4.8
Mean	95.8	17	8.1	82.52	93	16.59	80.8	62	19.7	91.3	25	19.4	91.2	28	19.7	93.5	21	17.9	94.2	20	10.8	

4.3.3 Assembly State Detection and 6D Pose Estimation

As shown in Table 3 and Table 2, ASDF shows promising results in terms of 6D pose estimation. Comparing the assembly state detection using the F1 score, see Table 4, shows that ASDF can predict the assembly state better (79.52) compared to a pure deep learning-based approach (73.85). Moreover, as denoted in Table 4, the 6D pose performance shows an improved performance by outperforming the deep learning-based approach in ADD(S) (95.74 (ours) compare to 84.92). Moreover, for the translation error we can reduce the average error by 14.2 mm.

For qualitative analysis we selected images from our test set, see Figure 5. It becomes apparent that, the state detection of ASDF is more precise compared to the deep learning-based approach. As shown in Figure 5 on different assemblies in different states (Screw Clamp) and unassembled (Nano Vise, Caliper) parts.

Moreover, we 3D printed the real-world assembly and manually annotated one sequence. As shown in Figure 5, our approach allows the detect the correct state during a real-world state transition.

4.4 GBOT Results

Existing approaches face the limitation of being either used for state detection combined with 2D object detection [32] or are limited to non accessible datasets [25, 38]. However, in terms of 6D pose estimation and 6D object tracking some approaches can handle 6D pose estimation for assembled parts. We focus on multi-state assembly comparisons, therefore, we omit comparing with single state approaches such as Mb-ICG [35], which require a re-initialization per assembly step. Our comparisons builds upon the

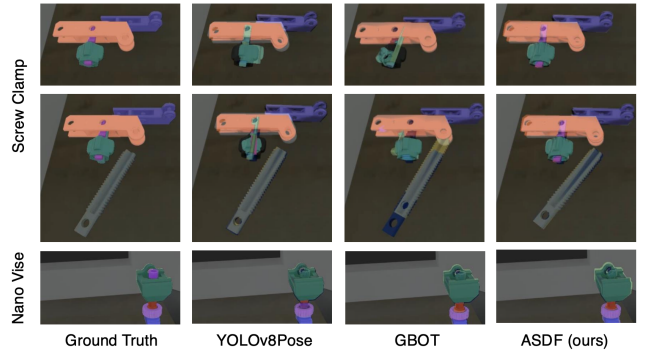


Figure 7: **Qualitative comparison of YOLOv8Pose [21], GBOT [21] and ASDF (ours) on the GBOT dataset:** We found that during assembly the results of ASDF are better compared to GBOT (Screw Clamp). Due to the improvement of pose refinement, ASDF performs better than YOLOv8Pose (Screw Clamp, Nano Vise).

benchmark proposed by Li et al. [21].

Given that we utilize the same objects as Li et al. [21], we assess our trained models from the ASDF dataset on the GBOT dataset without the need for retraining on their training set. We exclude the comparison with LiftPod since the screws and small connectors are excluded from their evaluation due to a category-level problem. As illustrated in Table 5, our approach demonstrates superior performance compared to GBOT and their fusion of GBOT with

deep learning-based re-initialization of object tracking. Moreover, in comparison to state-of-the-art tracking methods, Li et al. [21] introduce a deep learning-based approach for 6D pose estimation, which shares the same base architecture as our method. The outcomes presented in Table 5 shows that our approach, outperforms their deep learning baseline.

Furthermore, we conduct a visual comparison between our approach and GBOT, including their initialization network YOLOv8Pose, as depicted in Figure 7. The qualitative and quantitative analysis reveals that ASDF outperforms their deep learning-based and hybrid approach. Particularly, in the assembly process, ASDF exhibits notable improvements compared to GBOT.

5 DISCUSSION

ASDF shows more robust results compared to a pure deep learning-based approach on our ASDF and the GBOT dataset. Robust 6D pose estimation and assembly state detection allow adding visual overlays, e.g. see Figure 7 or even highlighting the current assembly state, see Figure 5. The more robust and correct the prediction is, the more reliably an AR interface can display this information.

Our evaluation has shown that combining object pose prediction with assembly state detection can lead to better results in 6D position estimation. However, the best performing approach is not always the most runtime friendly.

The assembly processes are complicated by occlusions and state changes. Previous work aimed at constant 6D position estimation of mounted objects using object tracking. However, they lack the additional state information [35, 21]. In addition, these approaches would have to reinitialize the tracking process in the event of occlusion. GBOT proposes the use of re-initialization with a real-time capable architecture. As the comparison with GBOT shows, we can even outperform their re-initialization approach in terms of 6D position estimation performance. This makes our work valuable in real-world scenarios.

The state transition, i.e. the change from state A to B, is a frequent challenge not only in the detection of assembly states. However, it is generally a challenge in phase detection or action detection [5]. A common approach in this regard, which is not considered in our evaluation, is to define a time frame between transitions, which is not considered in the evaluation. We did not do this as we were aiming for a real-world scenario where constant knowledge of the assembly state and object position is crucial. Therefore, we included these potentially error-prone parts in our dataset.

5.1 Limitations

In terms of performance we aimed for the highest accuracy. However, for the runtime this adds some additional overhead.

Moreover, the ASDF dataset features texture-less objects which do not propose the challenge of reflective materials such as medical instruments. Nevertheless, texture less objects propose a challenge.

The current approach focuses on reliable pose estimations and assembly state detection using a single camera and for the dataset on reproducible items. To address occlusion a multi-camera approach or even fusing static and dynamic camera input could provide additional information for the estimation.

6 CONCLUSION

We present ASDF a deep learning-based approach utilizing late fusion for assembly state detection and 6D pose estimation. ASDF can track objects from assembly state zero (unassembled) until the full assembly is completed. This enables smart guidance and can be used in the medical or industrial context. On our assembly dataset, we outperform the deep learning-based without a fusion step. Moreover, ASDF has demonstrated that awareness of the assembly state leads to an improved performance compared to the state-of-the-art in 6D pose estimation on the GBOT dataset. The

scenes in this dataset present various challenges, and ASDF has shown a huge improvement compared to YOLOv8Pose and outperformed all object tracking-based approaches.

In conclusion, our approach and dataset represent a promising step towards developing comparable backends for smart AR guidance in assembly processes.

ACKNOWLEDGMENTS

This work is funded by the German Federal Ministry of Education and Research (BMBF) with grant number 16SV8973.

We further thank d.hip for providing Hannah Schieber with a campus stipend.

REFERENCES

- [1] R. Alghonaim and E. Johns. Benchmarking domain randomisation for visual sim-to-real transfer. In *IEEE International Conference on Robotics and Automation (ICRA)*, 2021. 3, 5
- [2] A. Amini, A. Selvam Periyasamy, and S. Behnke. YOLOPose: Transformer-based multi-object 6d pose estimation using keypoint regression. In *Intelligent Autonomous Systems 17: Proceedings of the 17th International Conference IAS-17*, pp. 392–406. Springer, 2023. 2
- [3] Y.-W. Chao, W. Yang, Y. Xiang, P. Molchanov, A. Handa, J. Tremblay, Y. S. Narang, K. Van Wyk, U. Iqbal, S. Birchfield, and others. DexYCB: A benchmark for capturing hand grasping of objects. In *Proceedings of the IEEE/CVF Conference on Computer Vision and Pattern Recognition*, pp. 9044–9053, 2021. 3
- [4] E. Cramer, A. Kucharski, J. Kreimeier, S. Andreß, S. Li, C. Walk, F. Merkl, J. Högl, P. Wucherer, P. Stefan, et al. Requirement analysis for an ai-based ar assistance system for surgical tools in the operating room: stakeholder requirements and technical perspectives. *International Journal of Computer Assisted Radiology and Surgery*, pp. 1–10, 2024. 1, 2
- [5] K. C. Demir, H. Schieber, T. Weise, D. Roth, M. May, A. Maier, and S. H. Yang. Deep learning in surgical workflow analysis: a review of phase and step recognition. *IEEE Journal of Biomedical and Health Informatics*, 2023. 8
- [6] M. Denninger, M. Sundermeyer, D. Winkelbauer, D. Olefir, T. Hodan, Y. Zidan, M. Elbadrawy, M. Knauer, H. Katam, and A. Lodhi. BlenderProc: Reducing the reality gap with photorealistic rendering. In *Robotics: Science and Systems (RSS) Workshops*, 2020. 5
- [7] M. A. Fischler and R. C. Bolles. Random sample consensus: a paradigm for model fitting with applications to image analysis and automated cartography. *Communications of the ACM*, 24(6):381–395, 1981. 2
- [8] R. Girshick. Fast r-cnn. In *Proceedings of the IEEE international conference on computer vision*, pp. 1440–1448. IEEE/CVF, 2015. 2
- [9] A. Gupta, D. Fox, B. Curless, and M. Cohen. DuploTrack: a real-time system for authoring and guiding duplo block assembly. In *Proceedings of the 25th annual ACM symposium on User interface software and technology*, UIST '12, pp. 389–402. Association for Computing Machinery, 2012. doi: 10.1145/2380116.2380167 2
- [10] Y. He, H. Haibin, F. Haoqiang, C. Qifeng, and S. Jian. Ffb6d: A full flow bidirectional fusion network for 6d pose estimation. In *IEEE/CVF Conference on Computer Vision and Pattern Recognition*, 2021. 2, 3
- [11] S. J. Henderson and S. K. Feiner. Augmented reality in the psychomotor phase of a procedural task. In *2011 10th IEEE International Symposium on Mixed and Augmented Reality*, pp. 191–200, 2011. doi: 10.1109/ISMAR.2011.6092386 2
- [12] S. Hinterstoisser, V. Lepetit, S. Ilic, S. Holzer, G. Bradski, K. Konolige, and N. Navab. Model based training, detection and pose estimation of texture-less 3d objects in heavily cluttered scenes. In *Computer Vision—ACCV 2012: 11th Asian Conference on Computer Vision, Daejeon, Korea, November 5–9, 2012, Revised Selected Papers, Part I 11*, pp. 548–562. Springer, 2013. 5
- [13] T. Hodan, P. Haluza, S. Obdrzalek, J. Matas, M. Lourakis, and X. Zabulis. T-LESS: An RGB-d dataset for 6d pose estimation of texture-less

- objects. *IEEE Winter Conference on Applications of Computer Vision (WACV)*, 2017. 5
- [14] T. Hodan, J. Matas, and S. Obdrzalek. On evaluation of 6d object pose estimation. In G. Hua and H. Jegou, eds., *Computer Vision—ECCV 2016 Workshops: Amsterdam, The Netherlands, October 8–10 and 15–16, 2016, Proceedings, Part III 14*, vol. 9915, pp. 606–619. Springer International Publishing, 2016. doi: 10.1007/978-3-319-49409-8_52 5
- [15] T. Hodan, M. Sundermeyer, B. Drost, Y. Labbe, E. Brachmann, F. Michel, C. Rother, and J. Matas. BOP challenge 2020 on 6d object localization. *European Conference on Computer Vision Workshops (ECCVW)*, 2020. 3
- [16] G. Jocher, A. Chaurasia, and J. Qiu. YOLO by ultralytics, 2023. 2, 6
- [17] H. Jung, S.-C. Wu, P. Ruhkamp, G. Zhai, H. Schieber, G. Rizzoli, P. Wang, H. Zhao, L. Garattoni, S. Meier, D. Roth, N. Navab, and B. Busam. HouseCat6d – a large-scale multi-modal category level 6d object pose dataset with household objects in realistic scenarios, 2023. 2, 3
- [18] R. Kaskman, S. Zakharov, I. Shugurov, and S. Ilic. Homebreweddb: Rgb-d dataset for 6d pose estimation of 3d objects, 2019. 5
- [19] C. Kleinbeck, H. Schieber, S. Andress, C. Krautz, and D. Roth. ARTFM: Augmented reality visualization of tool functionality manuals in operating rooms. In *2022 IEEE Conference on Virtual Reality and 3D User Interfaces Abstracts and Workshops (VRW)*, pp. 736–737. IEEE, 2022. 1, 2, 3
- [20] V. Lepetit, F. Moreno-Noguer, and P. Fua. Ep n p: An accurate o(n) solution to the p n p problem. *International journal of computer vision*, 81:155–166, 2009. 2
- [21] S. Li, H. Schieber, N. Corell, B. Egger, J. Kreimeier, and D. Roth. GBOT: Graph-based 3d object tracking for augmented reality-assisted assembly guidance. In *2024 IEEE Conference Virtual Reality and 3D User Interfaces (VR)*, pp. 513–523. IEEE, 2024. 2, 3, 5, 7, 8
- [22] Y. Li, F. Zhong, X. Wang, S. Song, J. Li, X. Qin, and C. Tu. For a more comprehensive evaluation of 6dof object pose tracking, 2023. 7
- [23] H. Liu, Y. Su, J. Rambach, A. Pagani, and D. Stricker. Tga: Two-level group attention for assembly state detection. In *2020 IEEE International Symposium on Mixed and Augmented Reality Adjunct (ISMAR-Adjunct)*, pp. 258–263. IEEE, 2020. 2, 3, 5
- [24] F. Manuri, A. Pizzigalli, and A. Sanna. A state validation system for augmented reality based maintenance procedures. *Applied Sciences*, 9(10):2115, 2019. doi: 10.3390/app9102115 2
- [25] K. Murray, J. Schierl, K. Foley, and Z. Duric. Equipment assembly recognition for augmented reality guidance. In *2024 IEEE International Conference on Artificial Intelligence and eXtended and Virtual Reality (AIxVR)*, pp. 109–118. IEEE, 2024. 1, 2, 3, 5, 7
- [26] K. Park, T. Patten, and M. Vincze. Pix2pose: Pixel-wise coordinate regression of objects for 6d pose estimation. In *Proceedings of the IEEE/CVF International Conference on Computer Vision*, pp. 7668–7677, 2019. 2, 3
- [27] S. Peng, Y. Liu, Q. Huang, X. Zhou, and H. Bao. Pvnnet: Pixel-wise voting network for 6dof pose estimation. In *Proceedings of the IEEE/CVF Conference on Computer Vision and Pattern Recognition*, pp. 4561–4570. IEEE/CVF, 2019. 3
- [28] R. Radkowski. Object tracking with a range camera for augmented reality assembly assistance. *Journal of Computing and Information Science in Engineering*, 16(1):011004, 2016. 2
- [29] H. Schieber, K. C. Demir, C. Kleinbeck, S. H. Yang, and D. Roth. Indoor synthetic data generation: A systematic review. *Computer Vision and Image Understanding*, p. 103907, 2024. doi: 10.1016/j.cviu.2023.103907 3, 5
- [30] T. J. Schoonbeek, T. Houben, H. Onvlee, F. van der Sommen, et al. Industreal: A dataset for procedure step recognition handling execution errors in egocentric videos in an industrial-like setting. In *Proceedings of the IEEE/CVF Winter Conference on Applications of Computer Vision*, pp. 4365–4374, 2024. 3
- [31] T. J. Schoonbeek, T. Houben, H. Onvlee, P. H. N. d. With, and F. v. d. Sommen. IndustReal: A dataset for procedure step recognition handling execution errors in egocentric videos in an industrial-like setting, 2024. 3, 5
- [32] A. Stanescu, P. Mohr, M. Kozinski, S. Mori, D. Schmalstieg, and D. Kalkofen. State-aware configuration detection for augmented reality step-by-step tutorials. In *2023 IEEE International Symposium on Mixed and Augmented Reality (ISMAR)*, pp. 157–166. IEEE, 2023. 2, 3, 5, 7
- [33] M. Stoiber, M. Elsayed, A. E. Reichert, F. Steidle, D. Lee, and R. Triebel. Fusing visual appearance and geometry for multi-modality 6dof object tracking. In *2023 IEEE/RSJ International Conference on Intelligent Robots and Systems (IROS)*, pp. 1170–1177. IEEE, 2023. 2
- [34] M. Stoiber, M. Pfanne, K. H. Strobl, R. Triebel, and A. Albu-Schaeffer. SRT3d: A sparse region-based 3d object tracking approach for the real world. *International Journal of Computer Vision*, 130(4):1008–1030, 2022. 7
- [35] M. Stoiber, M. Sundermeyer, W. Boerdijk, and R. Triebel. A multi-body tracking framework—from rigid objects to kinematic structures, 2022. Publication Title: arXiv preprint arXiv:2208.01502. 2, 3, 7, 8
- [36] M. Stoiber, M. Sundermeyer, and R. Triebel. Iterative corresponding geometry: Fusing region and depth for highly efficient 3d tracking of textureless objects. In *IEEE/CVF Conference on Computer Vision and Pattern Recognition*, 2022. 2, 7
- [37] Y. Su, M. Liu, J. Rambach, A. Pehrson, A. Berg, and D. Stricker. IKEA object state dataset: A 6dof object pose estimation dataset and benchmark for multi-state assembly objects, 2021. Publication Title: arXiv preprint arXiv:2111.08614. 3
- [38] Y. Su, J. Rambach, N. Minaskan, P. Lesur, A. Pagani, and D. Stricker. Deep multi-state object pose estimation for augmented reality assembly. In *2019 IEEE International Symposium on Mixed and Augmented Reality Adjunct (ISMAR-Adjunct)*, pp. 222–227, 2019. doi: 10.1109/ISMAR-Adjunct.2019.00-42 2, 3, 5, 7
- [39] A. Tang, C. Owen, F. Biocca, and W. Mou. Comparative effectiveness of augmented reality in object assembly. In *Proceedings of the SIGCHI conference on Human factors in computing systems*, pp. 73–80, 2003. 2, 3
- [40] B. Tekin, S. N. Sinha, and P. Fua. Real-time seamless single shot 6d object pose prediction. In *Proceedings of the IEEE Conference on Computer Vision and Pattern Recognition (CVPR)*. IEEE/CVF, 2018. 2, 3
- [41] K. K. Thiel. *Automated Creation, Evaluation and Configuration of Markerless Object Tracking for Superimposed Augmented Reality*. PhD thesis, Technische Universität München, 2023. 3
- [42] J. Tobin, R. Fong, A. Ray, J. Schneider, W. Zaremba, and P. Abbeel. Domain randomization for transferring deep neural networks from simulation to the real world. In *2017 IEEE/RSJ International Conference on Intelligent Robots and Systems (IROS)*, pp. 23–30, 2017. doi: 10.1109/IROS.2017.8202133 3
- [43] J. Tremblay, A. Prakash, D. Acuna, M. Brophy, V. Jampani, C. Anil, T. To, E. Cameracci, S. Boochoon, and S. Birchfield. Training deep networks with synthetic data: Bridging the reality gap by domain randomization. In *Proceedings of the IEEE Conference on Computer Vision and Pattern Recognition (CVPR) Workshops*, 2018. 3
- [44] VisionLib. Showcase: Tracking multiple parts - visionlib. <https://www.youtube.com/watch?v=Gf06hmk7kww>, 2024. Accessed: 2024-06-26. 2
- [45] G. Wang, F. Manhardt, F. Tombari, and X. Ji. Gdr-net: Geometry-guided direct regression network for monocular 6d object pose estimation. In *Proceedings of the IEEE/CVF Conference on Computer Vision and Pattern Recognition*, pp. 16611–16621. IEEE/CVF, 2021. 2, 3
- [46] P. Wang, H. Jung, Y. Li, S. Shen, R. P. Srikanth, L. Garattoni, S. Meier, N. Navab, and B. Busam. PhoCaL: A multi-modal dataset for category-level object pose estimation with photometrically challenging objects. In *Proceedings of the IEEE/CVF Conference on Computer Vision and Pattern Recognition (CVPR)*, pp. 21222–21231, 2022. 2
- [47] R. Wang, Y. Zhang, J. Mao, R. Zhang, C.-Y. Cheng, and J. Wu. IKEA-manual: Seeing shape assembly step by step. In S. Koyejo, S. Mohamed, A. Agarwal, D. Belgrave, K. Cho, and A. Oh, eds., *Advances in Neural Information Processing Systems*, vol. 35, pp. 28428–28440. Curran Associates, Inc., 2022. 3
- [48] L.-C. Wu, I.-C. Lin, and M.-H. Tsai. Augmented reality instruction for object assembly based on markerless tracking. In *Proceedings of the*

- 20th ACM SIGGRAPH Symposium on Interactive 3D Graphics and Games, I3D '16, pp. 95–102. Association for Computing Machinery, 2016. doi: 10.1145/2856400.2856416 2
- [49] Y. Xiang, T. Schmidt, V. Narayanan, and D. Fox. PoseCNN: A convolutional neural network for 6d object pose estimation in cluttered scenes, 2017. Publication Title: arXiv preprint arXiv:1711.00199. 2, 3
- [50] M. Zaccaria, F. Manhardt, Y. Di, F. Tombari, J. Aleotti, and M. Giorgini. Self-supervised category-level 6d object pose estimation with optical flow consistency. *IEEE Robotics and Automation Letters*, 8(5):2510–2517, 2023. doi: 10.1109/LRA.2023.3254463 3
- [51] J. Zauner, M. Haller, A. Brandl, and W. Hartman. Authoring of a mixed reality assembly instructor for hierarchical structures. In *The Second IEEE and ACM International Symposium on Mixed and Augmented Reality, 2003. Proceedings.*, pp. 237–246, 2003. doi: 10.1109/ISMAR.2003.1240707 1, 2
- [52] Y. Zheng, Y. Kuang, S. Sugimoto, K. Astrom, and M. Okutomi. Revisiting the pnp problem: A fast, general and optimal solution. In *Proceedings of the IEEE International Conference on Computer Vision*, pp. 2344–2351, 2013. 2
- [53] B. Zhou and S. Güven. Fine-grained visual recognition in mobile augmented reality for technical support. *IEEE Transactions on Visualization and Computer Graphics*, 26(12):3514–3523, 2020. doi: 10.1109/TVCG.2020.3023635 2